PCCP

Accepted Manuscript

ROYAL SOCIETY OF CHEMISTRY

www.rsc.org/pccp

PCCP

ARTICLE

Light harvesting in photonic crystals revisited: why do slow photons at the blue edge enhance absorption?

Received 00th January 20xx,
Accepted 00th January 20xx

DOI: 10.1039/x0xx00000x

www.rsc.org/

O. Deparis,[a,*] S. R. Mouchet[a] and B.-L. Su[b]

Light harvesting enhancement by slow photons in photonic crystal catalysts or dye-sensitized solar cells is a promising approach for increasing the efficiency of photoreactions. This structural effect is exploited in inverse opal TiO_2 photocatalysts by tuning the red edge of the photonic band gap to the TiO_2 electronic excitation band edge. In spite of many experimental demonstrations, the slow photon effect is not fully understood yet. In particular, observed enhancement by tuning the blue edge has remained unexplained. Based on rigorous couple wave analysis simulations, we quantify light harvesting enhancement in terms of absorption increase at a specific wavelength (monochromatic UV illumination) or photocurrent increase (solar light illumination), with respect to homogeneous flat slab of equivalent material thickness. We show that the commonly accepted explanation relying on light intensity confinement in high (low) dielectric constant regions at the red (blue) edge is challenged in the case of TiO_2 inverse opals because of the sub-wavelength size of the material skeleton. The reason why slow photons at the blue edge are also able to enhance light harvesting is the loose confinement of the field, which leads to significant resonantly enhanced field intensity overlap with the skeleton in both red and blue edge tuning cases, yet with different intensity patterns.

Introduction

Slow photons are photons of wave-packets which travel at vanishing group velocity ($v_g = d\omega/dk \to 0$) in periodically structured optical media, i.e. photonic crystals, and, thanks to their long lifetime, interact efficiently with the material [1]. Slow photons appear at the lower (red) and higher (blue) frequency edges of the photonic band gap (PBG) where the electromagnetic field tends to concentrate in the high and low dielectric constant regions of the photonic crystal, respectively. According to this simplified picture, red edge slow photons are considered to be more useful for light harvesting enhancement and have been early exploited in order to increase the efficiency of photoreactions in inverse opal catalysts [2-5] and dye-sensitized solar cells [6-13]. Exploitation of the slow photon effect is more straightforward in photocatalysis than in photovoltaics because, in the latter case, charge carriers (electrons and holes) must be collected by electrodes for generating electrical current whereas, in the former case, they are readily available for redox reactions with adsorbed molecules. The present study is focused on titania (TiO_2) inverse opal photocatalysts, though the reported analysis could be transposed to solar cells.

Excellent photocatalytic performance of TiO_2 semiconductor material combined with its low fabrication cost and environmental safety make TiO_2-based photocatalysts a subject of intensive research and development [14] for hydrogen production [15] (water splitting) or photodegradation of volatile organic compounds [16-20] (water treatment, air purification). In comparison with the literature dedicated to electronic and chemical aspects of photocatalysts, less attention has been paid to light harvesting enhancement through structural effects, i.e. slow photon effect. The key concept behind this effect is the exploitation of the vanishing group velocity of slow photons and the tuning of their wavelength such that it overlaps with the electronic excitation wavelength of the semiconductor [3]. By doing so, optical absorption is enhanced due to the longer photon lifetime in the photonic crystal, giving rise to an increased number of photogenerated electron-hole pairs (excitons) and, eventually, to a higher photocatalytic activity [2-5]. Anatase nanocrystalline (nc) titania (TiO_2) is well known to give the best photocatalytic performance [18-21]. In this material, the electronic excitation wavelength (absorption band edge) is located around 370 nm [22], in the UV, which implies that nc-TiO_2 inverse opals must be designed in order to have their PBG below or above the UV-visible boundary, depending on which edge is selected. In heterogeneous photocatalysis, an open network of macropores is required so that reactants (gas or liquid) can have access to the high material specific area. In practice, connected pores can be achieved by rearrangement of spherical voids during the fabrication process [21]. The fabrication of TiO_2 inverse opals typically involves the following

[a] Solid-State Physics Laboratory, University of Namur, 61 rue de Bruxelles, B-5000 Namur, Belgium.
[b] Laboratory of Inorganic Materials Chemistry (CMI), University of Namur, 61 rue de Bruxelles, B-5000 Namur, Belgium.
* Email: olivier.deparis@unamur.be.

Electronic Supplementary Information (ESI) available: [details of numerical computation aspects is included]. See DOI: 10.1039/x0xx00000x

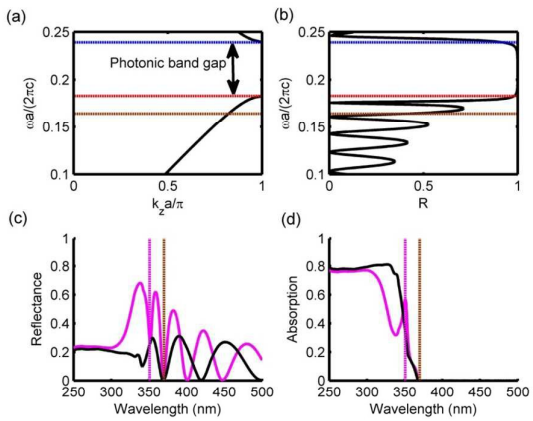

Fig. 1 (a) Photonic band diagram at normal incidence of infinite 1D photonic crystal (d_1=40.5 nm, d_2=0.5×d_1, n_1=2.8, n_2=1.33). (b) Reflectance spectrum of red-edge-tuned BR slab (d_1=40.5 nm, d_2=0.5×d_1, N=10) with TiO_2 extinction coefficient set artificially to zero. (c) Reflectance spectrum of the same slab as (b) but calculated with complex refractive index of anatase TiO_2. (d) Absorption spectrum of the same slab as (c). In (a, b), horizontal red (blue) dashed lines indicate red (blue) edge of the photonic band gap; horizontal brown dashed line indicates TiO_2 electronic band edge. In (c, d), vertical magenta (brown) dashed lines indicate red edge wavelength (TiO_2 electronic band edge wavelength). Normal incidence is assumed (incidence medium: water, substrate: glass). Reflectance and absorption spectra of the reference slab (black curves) are also shown (c, d).

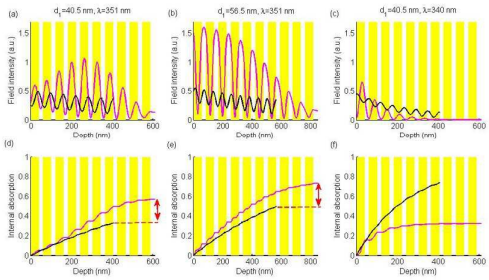

Fig. 2 Profiles of the field intensity (a, b, c) and the internal absorption (d, e, f) in BR slabs (magenta curves) and reference slabs (black curves). In (a, d) and (b, e), λ=351 nm and BR slabs were tuned such that, respectively, red and blue edge wavelengths were at λ=351 nm. In (c, f), λ=340 nm and the BR slab was red-edge tuned at λ=351 nm such that λ=340 nm was inside the photonic band gap. Calculations were done at normal incidence. Yellow rectangles in (a) indicate TiO_2 layers. Red arrows (d, e) indicate the absorption enhancement.

steps: synthesis of a close-packed opal template through self-assembly of e.g. polystyrene spheres, infiltration of the opal template with a TiO_2 precursor solution and sol-gel synthesis, thermal annealing to obtain the desired crystalline phase of TiO_2, and finally calcination to remove the spheres [21]. During this final step, the sphere diameter shrinks to some extent, leaving an open macroporous network [21]. Due to uncertainty in the amount of sphere shrinking, it is difficult to target either red or blue edge tuning by choosing of the diameter of the template spheres. In practice, tuning of the PBG edges is achieved by changing the incidence angle [21].

In photocatalysis experiments, monochromatic UV sources or polychromatic (white light) sources are used for illumination. In real-world applications, solar light is used. Under polychromatic illumination, the photogenerated current density is given by [7]: $J = e/hc \int \eta\lambda A(\lambda) S(\lambda) d\lambda$, where e is the electron charge, h is the Planck's constant, c is the speed of light in vacuum, η is the internal quantum efficiency (assumed to be equal to unity†), λ is the wavelength, $A(\lambda)$ is the catalyst absorption spectrum and $S(\lambda)$ is the AM1.5 (at earth, mid latitudes) solar irradiance spectrum. All incident photons with energies higher than the TiO_2 electronic band edge contribute to the photocurrent, although higher energy photons have a lower weight (cf. factor λ in the integrand). In principle, there is room for absorption enhancement over a broad spectral range, from the solar spectrum UV cut-off wavelength (280 nm) to the TiO_2 absorption cut-off wavelength (370 nm). However, the slow photon effect enhances absorption within a rather narrow spectral band and competes with other photonic effects (PBG reflection) which reduce absorption [2]. Therefore, in general, care should be taken to optimize the photonic crystal with respect to photocurrent and not only to absorption at a specific wavelength, unless a monochromatic source is used.

Since slow photons are associated with the confinement of the electromagnetic field intensity in regions of high (low) dielectric constant around the red (blue) edge wavelengths, it sounds obvious to select the red edge for exploiting the slow photon effect in inverse opals. Indeed, the blue edge does not seem relevant since it would lead to confinement in the spherical voids. Experimental works, however, reported enhanced photocatalytic activity for both red and blue edge tuning [21]. Early numerical simulations showed also enhanced absorption in dye-sensitized solar cells at both blue and red edges, though without addressing the peculiarity of the blue edge case [7]. These puzzling results call for revisiting the understanding of the slow photon effect. In this article, we show that the commonly accepted explanation relying on light intensity confinement in high dielectric constant regions at the red edge is challenged in the case of inverse opals because of the sub-wavelength size of the material skeleton. To demonstrate this statement, we resort to numerical electromagnetic simulations, which have proven to be an efficient design tool in various applications of photonic crystals.

Numerical simulations

Photonic crystal models

Photonic-crystal-based catalysts built from anatase TiO_2 (active material) and void spaces (pores) are considered throughout the following. For efficient photoreactions, the macroporous network must be open (i.e. interconnected pores), as mentioned above. Face centered cubic (f.c.c.) inverse opal (IO) structures with TiO_2 volume filling fraction (f) lower than the close packing value (f=26%) meet this open porosity requirement. Nonetheless, we will begin our analysis by considering a unidimensional (1D) photonic crystal, i.e. Bragg reflector (BR) or periodic stack of alternating TiO_2 and void layers. As a catalyst, this structure is hardly realizable since it would require some support systems for void layers which would not anyway be accessible for reactants unless some complications are added to the design. In spite of these practical aspects, the study of planar structures allows us to gain a preliminary understanding of the slow photon effect, which will be further developed in the case of inverse opals.

As a typical example of applications, we considered heterogeneous photocatalysis in aqueous phase. Water (refractive index: n_{water}=1.33) was taken as the incidence medium in all optical simulations. It was further assumed that water filled all the voids of the photonic crystal structure, thereby reducing the refractive index contrast with TiO_2 as compared to air. All the studied photonic crystals were assumed to take the form of slabs of finite thickness which laid on a semi-infinite glass substrate (refractive index: n_{glass}=1.50). The optical properties of anatase TiO_2 were modelled using optical constant data reported in the literature [10]. The material absorption was accounted by the imaginary part of the complex refractive index, i.e. the extinction coefficient k. From the wavelength dependence of k (see **Fig. S1**, Electronic Supplementary Information), the electronic excitation cut-off wavelength (absorption band edge) was estimated to be about 370 nm. The parameters of BR slabs were: TiO_2 layer thickness (d_1), water-filled void layer thickness (d_2), unit cell period (a=d_1+d_2), number of periods (N). The parameters of IO slabs were: spherical void diameter (D), TiO_2 volume filling fraction (f), f.c.c. lattice constant (ac), number of unit cells (N). The IO crystal was assumed to be oriented such that the (111) crystallographic direction was perpendicular to the slab surface. The lattice constant and the unit cell length along (111) direction were determined from the sphere diameter and the filling fraction as follows: $a_c = D(3f/2\pi)^{-1/3}$ and $a_c\sqrt{3}$, respectively. Open porosity (connected network of voids) required $f \leq 0.26$.

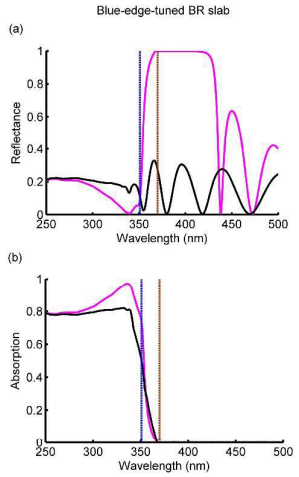

Fig. 3 (a) Reflectance spectrum of blue-edge-tuned BR slab (d_1=56.5 nm, d_2=0.5×d_1, N=10). (d) Absorption spectrum of the same slab as (a). Vertical blue (brown) dashed lines indicate blue edge wavelength (TiO_2 electronic excitation wavelength). Normal incidence was assumed (incidence medium: water, substrate: glass). Reflectance and absorption spectra of the reference slab (black curves) are also shown.

Computational methods

Reflectance and absorption spectra of TiO_2 inverse opal slabs were calculated using the rigorous coupled wave analysis (RCWA) method [23-25] implemented in a home-made code. The code allowed us to calculate also the electromagnetic field at any point inside the photonic structure, in particular to draw maps and profiles of the field intensity, i.e. $I(\vec{r}) \div |E(\vec{r})|^2$. The RCWA method solves Maxwell's equation without any approximation and is based on Fourier series expansion of laterally periodic permittivity, i.e. $\epsilon(\vec{r}) = \epsilon(x + pR_x, y + qR_y)$ ($\vec{R}$: lateral translation vector, p, q: integer numbers), as well as corresponding expansions of the fields according to Bloch-Floquet theorem [23-25]. For this reason, the IO slab had to be discretized into layers in which ε was constant along z axis (see **Fig. S2**, Electronic Supplementary Information). Although there is no approximation in RCWA, its implementation in a computer code requires using a finite number of Fourier coefficients which introduces a numerical truncation error[‡]. It is noteworthy that RCWA fully accounts for multiple scattering propagation of light wave in three-dimensional photonic structures [23-25]. The concept of local absorption [26] was found to be useful for our analysis. The local absorption was calculated directly from the computed field intensity at a given point and the imaginary part of the (Fourier reconstructed) permittivity at the same point: $A_{\mathrm{loc}}(\vec{r}) \div \Im\epsilon(\vec{r}) \times I(\vec{r})$. Since only the TiO_2 skeleton was absorbing, field intensity localized inside the voids was useless. The photonic band diagram (i.e. dispersion relation) of close-packed (f=0.26) TiO_2 inverse opals was calculated using the MIT Photonic-Bands package (MPB) [27]. For this calculation, the refractive indexes of titania, water and air were taken equal to 2.7, 1.33 and 1.00, respectively. Finally, for BR slabs, the photonic band diagram, reflectance and absorption spectra were calculated using the 1D transfer-matrix method [28]. The concept of internal absorption [29], i.e. absorption cumulated up to a given depth inside the layered structure, was found to be useful in this case.

Reference and enhancement factors

A fair evaluation of light harvesting enhancement in photonic crystal catalysts required comparison with a reference. We defined as reference an equivalent homogeneous slab of thickness (d_{ref}) such that the quantity of TiO_2 material per unit area was the same as in the photonic crystal ($d_{ref}=d_1\times N$ for BR slabs, $d_{ref}=N\times a_c\times f$ for IO slabs). Based on this reference, we defined two enhancement factors. The first one pertained to monochromatic illumination and was defined as the ratio between photonic crystal and reference absorption values at the excitation wavelength. The second one pertained to solar illumination and was defined as the ratio between photonic crystal and reference photocurrent values. It is noteworthy that the calculated photocurrent value took into account spectral dependences of both the solar radiation and the slab absorption.

Results and discussion

Revisiting the slow photon effect in 1D photonic crystals

The existence of a photonic band gap arises from the periodic alternation in space of regions of high and low permittivity ϵ (or refractive index $n=\sqrt{\epsilon}$). The simplest realization of a PBG material is the Bragg reflector, known for about a century before the advent of photonic crystals. The current explanation of the slow photon effect in TiO_2 inverse opal catalysts relies on the simplified picture of light intensity confinement in TiO_2 regions at wavelengths near the PBG red edge, which leads to enhanced absorption as far as the red edge is tuned to the electronic excitation wavelength of TiO_2. Such an interpretation is reminiscent of the analysis of slow light propagation in a 1D photonic crystal. As a matter of fact, slow light propagation in 3D photonic crystals, such as inverse opals, is much more complicated than in 1D photonic crystals, where scattering occurs at interfaces between planar layers.

In order to put to the test the above mentioned interpretation, let us first consider the case of an infinite 1D photonic crystal and its finite realization, a BR slab on a glass substrate.

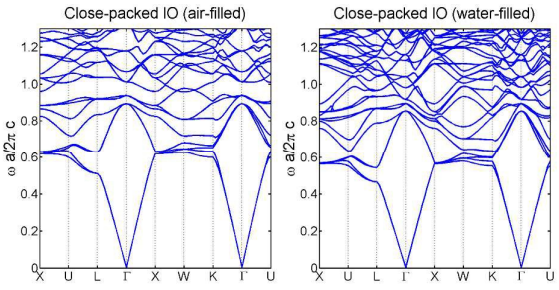

Fig. 4 Photonic band diagrams of close-packed TiO_2 inverse opals with spherical voids filled with air (left) or water (right) Refractive indexes: n=2.7 (TiO_2), n=1.33 (water), n=1.0 (air). Note a pseudo PBG at L point of the irreducible Brillouin zone. In MPB code, 64×64×64 plane waves were used in the Fourier expansions of the electromagnetic field and the dielectric constant.

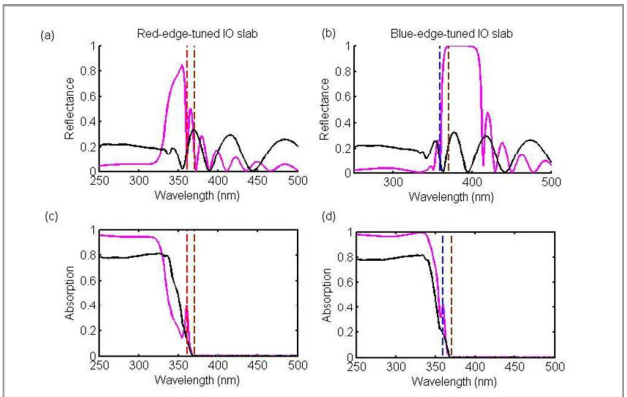

Fig. 5 Reflection (a, b) and absorption (c, d) of close-packed IO slabs with D=115 nm (a, c) and D=137 nm (b, d). Vertical red (blue) dashed lines indicate positions of red (blue) edge wavelength. Non-polarized light incident along (111) crystallographic direction (polar angle θ=0°, azimuthal angle ϕ=-30°). Reflectance and absorption spectra of reference slabs are also shown.

Without loss of generality, water-filled void layers were chosen to be half thinner than TiO_2 layers ($d_2=0.5\times d_1$). Non-polarized light was assumed to impinge on the stack at normal incidence. In the photonic band diagram of the infinite 1D photonic crystal, vanishing group velocity occurred at the blue (high) and red (low) frequency edges of the PBG (**Fig. 1a**). The reflectance spectrum of a hypothetical non-absorbing BR slab (real wavelength-independent refractive index) is shown in **Fig. 1b** for N=10 bilayers. Note that the positions of red and blue edge frequencies were well approximated by the positions of the first reflectance minima on both sides of the Bragg peak (these minima got closer to the edges as N was increased). The layer thicknesses were chosen such that, in wavelength units, the red edge (~351 nm) was located slightly below the TiO_2 electronic band edge (~370 nm). Reflectance and absorption spectra of the same BR slab in which material absorption was taken into account (through complex wavelength-dependent refractive index) are shown in **Fig. 1c** and **Fig. 1d**, together with spectra of the reference slab. Note that thin film interferences in the reference slab and Bragg peak in the BR slab were damped (**Fig. 1c**) due to strong TiO_2 absorption below 370 nm (**Fig. S1**). In comparison with the reference slab, the BR slab exhibited enhanced absorption around the red edge (**Fig. 1d**). It was no surprise since, in a BR slab at red edge frequency, light intensity tends to concentrate in the high-index layers [1], as observed in the field intensity profile (**Fig. 2a**). Since the high-index layers were made of TiO_2, the field confinement in these layers explained the observed enhancement. As slow light tunneled through the photonic crystal, it was resonantly absorbed in TiO_2 layers and the internal absorption exceeded that in the reference slab (**Fig. 2d**).

At blue edge frequency, on the other hand, light intensity tended to concentrate in the low-index layers (**Fig. 2b**), which was at first glance not favorable at all for enhancing absorption. However, we found that blue edge tuning (**Fig. 3a**)

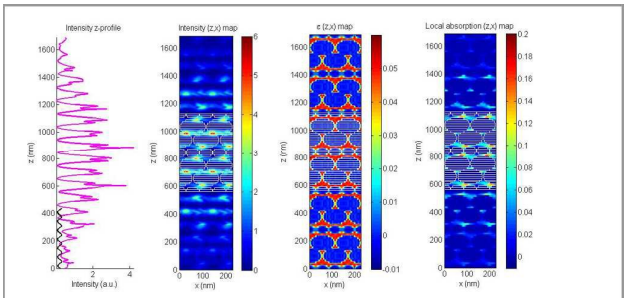

Fig. 6 (From left to right) Intensity *z*-profile at the center of unit cell (magenta curve) and cross section (*x*,*z*) maps of field intensity, imaginary part of dielectric constant and local absorption in a close-packed IO slab with *D*=115 nm (red-edge-tuned). Profiles and maps were calculated at λ=361 nm for non-polarized light impinging perpendicularly to the slab. Sphere cross sections are shown in the central part of the IO slab as guide for the eyes. Intensity *z*-profile in the reference slab is also shown (black curve).

also resulted in absorption enhancement (**Fig. 3b**). This apparently surprising result could be explained as follows: in spite of the fact that field intensity maxima were located in the void layers (**Fig. 2b**) the field intensity was higher *on average* than in the reference slab. As a consequence, the internal absorption was enhanced (**Fig. 2e**). This previously unnoticed effect should remain valid in 3D photonic crystals and could explain intriguing experimental observations of enhanced photocatalytic activity in blue-edge-tuned TiO_2 inverse opals [21].

Absorption/photocurrent enhancement in 1D photonic crystals

In both red-edge-tuned and blue-edge-tuned BR slabs, absorption was enhanced around the same wavelength as a result of our choice of the unit cell period ($a=d_1+d_2$). Enhancement factor (at 351 nm) were equal to 1.72 and 1.47, respectively (**Fig. 2**). Note that the absolute absorption levels were different since the total TiO_2 thicknesses ($N\times d_1$) were different. In the red-edge-tuned BR slab, the band gap reflection at shorter wavelengths was responsible for a strong decrease of the absorption, which felt below the reference between about 300 nm and 345 nm. Consequently, although the absorption was resonantly enhanced close to the TiO_2 electronic band edge, the photocurrent was reduced (J=1.18 mA/cm²) w.r.t. reference (J=1.42 mA/cm²). This detrimental effect was not encountered in the blue-edge-tuned BR slab since the PBG was located above the TiO_2 electronic excitation cut-off wavelength. As a result, the photocurrent was enhanced (J=1.67 mA/cm²) w.r.t. reference (J=1.49 mA/cm²) by a factor equal to 1.12. In accordance with early reports on inverse opal catalysts [2-4], we note that overlap between PBG and light source spectrum should be avoided. Indeed, when the incident wavelength was inside PBG, the field intensity decayed rapidly with depth (**Fig. 2c**) and the internal absorption saturated accordingly to a level lower than the reference (**Fig. 2f**). As far as solar light illumination is concerned, red edge tuning is not appropriate since the PBG prevents light entering into the structure at shorter wavelengths, thereby reducing the absorption in a substantial part of the solar UV spectrum. On the contrary, red-edge tuning leads to the best performance when it matches the monochromatic excitation wavelength. Although not coined so far, blue edge tuning can also lead to enhanced absorption in BR slabs. This important conclusion will be re-examined hereafter in the case of inverse opals.

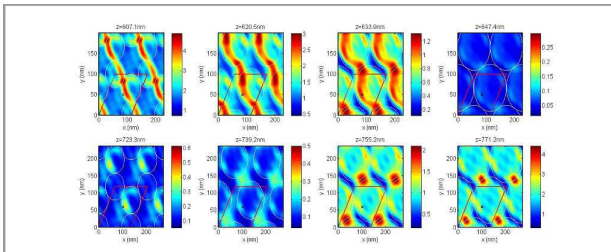

Fig. 7 Cross section (*x*,*y*) maps of field intensity at various depths in red-edge-tuned (top row) and blue-edge-tuned (bottom row,) close-packed IO slabs with, respectively, D=115 nm and *D*=137 nm. Maps were calculated at λ=361 nm (top row) and λ=359 nm (bottom row) for non-polarized light impinging perpendicularly to the slab. Cross section (centre) of the unit cell is indicated by red parallelogram (black cross). White circles are sphere cross sections.

The slow photon effect in inverse opals

The photonic band diagrams of close-packed TiO_2 inverse opals with either water or air filling the voids (**Fig. 4**) show that they possess, among others, a pseudo PBG at the L point of the irreducible Brillouin zone, notably along the ΓL direction, i.e. (111) crystallographic direction. The size of the gap reduces and its edges move to lower normalized frequencies ($\Omega=a_c\omega/2\pi c=a_c/\lambda$) when water replaces air inside the spherical voids.

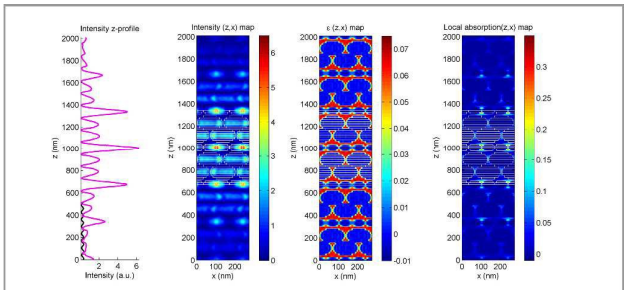

Fig. 8 (From left to right) Intensity *z*-profile at the center of unit cell (magenta curve) and cross section (*x*,*z*) maps of field intensity, imaginary part of dielectric constant and local absorption in a close-packed IO slab with *D*=137 nm (blue-edge-tuned). Profiles and maps were calculated at λ=359 nm for non-polarized light impinging perpendicularly to the slab. Sphere cross sections are shown in the central part of the IO slab as guide for the eyes. Intensity *z*-profile in the reference slab is also shown (black curve).

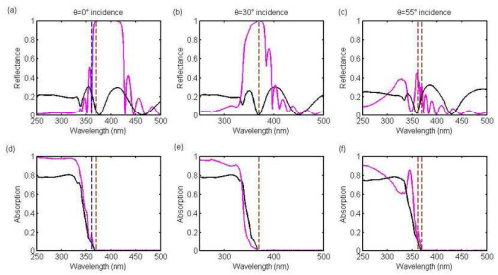

Fig. 9 Reflection (a, b, c) and absorption (d, e, f) of IO slab with D=167 nm and *f*=0.12 (open porosity). Vertical red (blue) dashed lines indicate positions of red (blue) edge of the photonic band gap. Non-polarized light, ϕ=-30°, θ=0° (a, d), θ=30° (b, e), θ=55° (c, f). For comparison, reflectance and absorption spectra of reference slabs are also shown.

We first analysed the slow photon effect in close-packed (*f*=0.26) inverse opals. The (111)-cut IO slabs consisted of *N*=6 unit cells (thickness: $d_{\mathrm{IO}} = Na_{\mathrm{c}}\sqrt{3}$ with a_{c} the lattice constant). Non-polarized, normally incident light was assumed. The normal incidence direction corresponded to the ΓL direction in reciprocal space. When the sphere diameter was chosen to be *D*=115 nm (d_{IO}=1.690 μm), the red edge was tuned to 361 nm, slightly below the TiO_2 electronic band edge, as it can be observed in the reflectance spectrum (**Fig. 5a**). An absorption enhancement factor equal to 3.09 was obtained at 361 nm (**Fig. 5c**). The photocurrent was slightly higher (*J*=1.46 mA/cm²) w.r.t reference (*J*=1.45 mA/cm²) because the PBG reflection (**Fig. 5a**) decreased the absorption between 330 nm and 350 nm (**Fig. 5c**). When the sphere diameter was chosen to be *D*=137 nm (d_{IO}=2.014 μm), the blue edge was tuned to 359 nm (**Fig. 5b**). An absorption enhancement factor equal to 2.23 (lower than for the red edge) was obtained at 359 nm (**Fig. 5d**). The photocurrent was significantly higher (*J*=1.85 mA/cm²) w.r.t. reference (*J*=1.47 mA/cm²) because the PBG reflection occurred above the TiO_2 electronic bad edge (**Fig. 5b**). The photocurrent enhancement factor was equal to 1.25 in this case.

Computed field tomography in inverse opals

Computed tomography of the field intensity (and local absorption) turned out to be very useful for better understanding the slow photon effect. In tomographic representation, the *z*-coordinate was taken along the (111) direction, normal to the slab surface and intersecting the (*x*,*y*) plane at the center (x_0,y_0) of the unit cell. The numerical accuracy of *x* and *y* positions was set by the computing grid. Afforded computing time limited the grid resolution to 40×40 points, i.e. accuracy of about 5 nm. The same constraint limited the accuracy on *z* position (about 4 nm). The accuracy on intensity values was only limited by computer precision. It is noteworthy that a complete field tomography, *I*=*I*(*x*,*y*,*z*), is not accessible to experiments, which makes all the interest of simulations for understanding phenomena such as light localization in complex 3D structures. The (*x*,*z*) map of the field intensity in $y=y_0$ cross section plane showed that, in the red-edge tuned IO slab, the intensity was predominantly concentrated in the TiO_2 skeleton and higher in the central region of the slab (**Fig. 6**). Red edge slow photons tunneled across the IO structure and experienced resonantly enhanced intensity w.r.t. wave propagation in a homogenous medium (reference slab). Only intensity located in the skeleton gave rise to absorption, as it can be seen in the local absorption (*x*,*z*) map (**Fig. 6**). The latter was computed using the Fourier reconstruction of the imaginary part $\Im\epsilon(\vec{r})$ of the spatially varying dielectric constant (**Fig. 6**). From the reconstructed map, it was clear that the IO structure was reproduced with high fidelity, i.e. $\Im\epsilon(\vec{r})$ was zero inside spheres and quite uniform inside the TiO_2 skeleton with values close to the expected value at the selected wavelength. Numerical noise arising from Fourier reconstruction reduced slightly the image quality of local absorption maps. The (*x*,*y*) maps of the field intensity in various transversal cross section planes helped refining the analysis (**Fig. 7**, top row). In cross sections where the skeleton formed a connected network (voids were close to each other but did not touch), the field spread on both skeleton and voids but had some local maxima overlapping the skeleton. In cross sections where the skeleton was made of isolated islands, the field tended to concentrate in the voids. From the above analysis, it is clear that the assumption of field confinement in the high-ε regions at red edge is far from being valid to describe the actual field tomography. The reason lies in the sub-wavelength size of the TiO_2/void regions which leaves no room to the field but to extend over both regions. In other words, loose confinement challenges the common interpretation of the slow photon effect.

In the blue-edge-tuned IO slab, the intensity was mostly concentrated in the voids and is higher in the central region of the slab (**Fig. 8**). However, the field extended into the TiO_2 skeleton as well so that absorption took place locally there (**Fig. 8**). The intensity *z*-profile confirmed that the intensity was, on average, strongly enhanced w.r.t reference (**Fig. 8**). This is an important result. Indeed, it demonstrates that absorption enhancement in inverse opals is also possible at the blue edge. Like the red edge slow photons, blue edge slow photons tunneled across the IO structure and experienced resonantly enhanced intensity tough in different patterns. Because of loose confinement, significant field overlap with

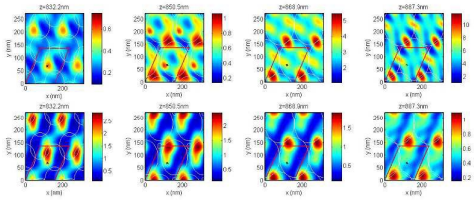

Fig. 10 Cross section (x,y) maps of field intensity in IO slab with D=167 nm, f=0.12 (open porosity) at incident polar angle θ=0° (top row, λ=361 nm) and θ=55° (bottom row, λ=362 nm). Cross section (center) of the unit cell is indicated by red parallelogram (black cross). Cross sections of spheres are indicated by white circles.

the TiO_2 skeleton led to absorption enhancement. This explanation was confirmed by cross section (x,y) maps (**Fig. 7**, bottom row), where the field had maxima into the connected-like skeleton whereas it concentrated inside voids of the island-like skeleton.

Finally, we analyzed the case of inverse opals with open porosity ($f \leq 0.26$). We simulated typical experiments [21] by using an IO slab with D=167 nm and f=0.12 (d_{IO}=2.317 μm) as well as by varying the incident polar angle (the incident azimuthal angle was fixed to ϕ=-30° in order to scan the photonic band diagram from ΓL to ΓU directions, **Fig. 4**). The sphere diameter was chosen such that it corresponded to blue edge tuning at normal incidence (θ=0°), as it can be noticed from the reflectance spectrum (**Fig. 9a**). Absorption enhancement factor equal to 2.37 was obtained at 361 nm in this case (**Fig. 9d**). As the incidence angle was increased (moving from ΓL to ΓU directions), the photonic band gap shifted towards shorter wavelengths (i.e. higher frequencies, see **Fig. 4**). At ϕ=30°, high PBG reflection (**Fig. 9b**) prevented light from entering the IO slab, thereby reducing the absorption (**Fig. 9e**) w.r.t. reference. Increasing the angle further to θ=55° led to red edge tuning (**Fig. 9c**) and an absorption enhancement factor equal to 2.49 was obtained at 362 nm (**Fig. 9f**). Analysis of the intensity maps in various layers (**Fig. 10**) confirmed the revisited explanation of the slow photon effect given above in the case of close-packed IO slabs, i.e. loose confinement leading to field overlap with TiO_2 skeleton. It is noteworthy that open porosity resulted in a thinner skeleton, which rendered field confinement in the skeleton more loose. In terms of photocurrent, both blue and red edge angle tuning led to higher values (J=1.66 mA/cm² and J=1.42 mA/cm², respectively) than reference (J=1.34 mA/cm² and J=1.33 mA/cm², respectively), with enhancement factors of 1.12 and 1.01, respectively.

The reliability of our simulations was assessed in a previous work [21], where the photonic band edges of anatase nc-TiO_2 inverse opal films of various sphere diameters were tuned by varying the incidence angle and photodegradation of Rhodamine B in aqueous solution was observed under UV-visible light exposure. Our prediction that, under solar light illumination, blue edge tuning leads to better light harvesting (higher photocurrent) than red edge tuning agrees nicely with higher photocatalytic activity observed in the former case [21].

Conclusions

We have theoretically investigated the origin of light harvesting enhancement in TiO_2 photonic crystal catalysts due to the slow photon effect. Although absorption enhancement of blue edge photons was previously observed in inverse opals, it was not rationalized. Even in the simple case of TiO_2/void Bragg stacks, our analysis revealed a previously unnoticed yet important aspect of 1D photonic crystals: the fact that blue edge photons can also experience enhanced absorption. This result led us to revisit the common interpretation of the slow photon effect in TiO_2 inverse opals. We showed that not only red but also blue edge tuning led to enhanced absorption because, due to loose confinement, the resonantly enhanced field intensity overlapped the TiO_2 skeleton in both cases, yet with different intensity patterns. The simplified picture of field confinement in low(high)-ϵ regions at blue (red) edge was found to be challenged in inverse opals because the material skeleton was so thin that field confinement in sub-wavelength size regions became looser and looser. We believe our theoretical results will help improving photocatalytic activity of inverse opals but also will induce new developments in other related fields such as photovoltaics.

Acknowledgements

S.M. was supported by the Belgian National Fund for Scientific Research (F.R.S.-FNRS) as Research Fellow. The authors acknowledge the use of resources of the "Plateforme Technologique de Calcul Intensif (PTCI)" (http://www.ptci.unamur.be) located at the University of Namur, which is supported by F.R.S.-FNRS under the convention No. 2.4520.11. The PTCI is member of the "Consortium des Équipements de Calcul Intensif (CÉCI)" (http://www.ceci-hpc.be).

Notes and references

† Assuming η=1, the calculated J value represents the maximal photocurrent that is achievable if each photogenerated electron/hole pair (exciton) is dissociated. In TiO_2-based catalysts, the internal quantum efficiency η is low because excitons can recombine before they are consumed in redox reactions. Because the scope of this article is to address the slow photon effect in general, without restriction to a specific catalyst material, we assumed η=1 as a theoretical limit which could be approached with, e.g., nanocomposite TiO_2 in which rapid transfer of electrons from/to nanoparticles effectively separates the photogenerated charges [30-32]. It is noteworthy that taking η<1 would only scale down J values, without changing the conclusions of the present study.

‡ The IO unit cell was divided into 21 layers (spherical voids approximated by stacks of cylinders), each layer being divided into 4 identical computational slices (thickness lower than $\sim\lambda/10$). The total number of Fourier coefficients $N_g=P\times Q$ (P, Q: numbers of coefficients along x and y axes) corresponded to retained diffraction orders (P=Q was taken because of symmetry). The choice of N_g resulted from a trade-off between computational time and fidelity in reconstructing $\epsilon(\vec{r})$ from Fourier series, which ensured numerical convergence (note that numerical noise arising from Fourier reconstruction reduced slightly the image quality of local absorption maps, **Fig. 6** and **Fig. 8**). For close-packed IO slabs, N_g=9×9=81 diffraction orders were used. Using N_g>81 led to computational instabilities due to high values of $\Im\epsilon(\vec{r})$ below TiO_2 absorbing spectral region. With N_g=81, the spatial dependence of both real and imaginary parts of ε could be reproduced with high fidelity. For IO slabs with connected pore network (interpenetrating spheres), N_g had to be restricted to N_g=5×5=25 due to an additional constraint related to our analytical Fourier treatment of intersecting permittivity islands. Nevertheless, computational accuracy and ε-reconstruction fidelity were found to be still acceptable.

1 J. D. Joannopoulos, R. D. Meade and J. N. Winn, *Photonic Crystals: Molding the Flow of Light* (Princeton, 1995).

2 J. I. L. Chen, G. von Freymann, S. Y. Choi, V. Kitaev, G. A. Ozin, *Adv. Mat.*, 2006, **18**, 1915.
3 J. I. L. Chen, G. von Freymann, S. Y. Choi, V. Kitaev and G. A. Ozin, *J. Mat. Chem.*, 2008, **18**, 369.
4 J. I. L. Chen and G. A. Ozin, J. Mat. Chem., 2009, **19**, 2675.
5 M. Wu, Y. Li, Z. Deng and B.-L. Su, ChemSusChem., 2011, **4**, 1481.
6 S. Nishimura, N. Abrams, B. A. Lewis, L. I. Halaoui, T. E. Mallouk, K. D. Benkstein, J. van de Lagemaat, A. J. Frank and *J. Am. Chem. Soc.*, 2003, **125**, 6306.
7 A. Mihi, H. Miguez, *J. Phys. Chem. B*, 2005, **109**, 15968.
8 S.-H. A. Lee, N. M. Abrams, P. G. Hoertz, G. D. Barber, L. I. Halaoui and T. E. Mallouk, *J. Phys. Chem. B*, 2008, **112**, 14415.
9 C.-H. Yip, Y.-M. Chiang and C.-C. Wong, J. Phys. Chem. C, 2008, **112**, 8735.
10 I. Rodriguez, F. Ramiro-Manzano, P. Atienzar, J. M. Martinez, F. Meseguer, H. Garcia and A. Corma, J. Mater. Chem., 2007, **17**, 3205.
11 L. I. Halaoui, N. M. Abrams and Thomas E. Mallouk, J. Phys. Chem. B, 2005, **109**, 6334.
12 P.R. Somani, C. Dionigi, M. Murgia, D. Palles, P. Nozar and G. Ruani, Solar Energy Mat. & Solar Cells, 2005, **87**, 513.
13 C. L. Huisman, J.Schoonman and A. Goossens, Solar Energy Mat. & Solar Cells, 2005, **85**, 115.
14 H. Xu, S. Ouyang, L. Liu, P. Reunchan, N. Umezawa and J. Ye, *J. Mater. Chem. A*, 2014, **2**, 12642.
15 G. I. N. Waterhouse, A. K. Wahab, M. Al-Oufi, V. Jovic, D. H. Anjum, D. Sun-Waterhouse, J. Llorca and H. Idriss, Sci. Rep., 2013, **3**, 2849.
16 Y. Donga, Y. Wanga, T. Cai, L. Kou, G. Yang and Z. Yan, Ceram. Int., 2014, **40**, 11213.
17 S.-L. Chen, A.-J. Wang, C. Dai, J. B. Benziger and X.-C. Liu, Chem. Eng. J., 2014, **249**, 48.
18 M. Wu, J. Liu, J. Jin, C. Wang, S. Huang, Z. Deng, Y. Li and B.-L. Su, Appl. Cat. B, 2014, **150-151**, 411.
19 M. Wu, A. Zheng, F. Deng and B.-L. Su, Appl. Cat. B, 2013, **138-139**, 219.
20 X. Li, L.-H. Chen, J. C. Rooke, Z. Deng, Z.-Y. Hu, S.-Z. Wang, L. Wang, Y. Li, A. Krief and B.-L. Su, J. Colloid Interface Sci., 2012, **394**, 1, 252.
21 M. Wu, J. Jin, J. Liu, Z. Deng, Y. Li, O. Deparis and B.-L. Su, *J. Mater. Chem. A*, 2013, **1**, 15491.
22 Y. R. Park and K. J. Kim, *Thin Solid Films*, 2005, **484**, 34.
23 J.-P. Vigneron, F. Forati, D. André, A. Castiaux, I. Derycke, and A. Dereux, *Ultramicroscopy*, 1995, **61**, 21.
24 J. B. Pendry, *Journal of Modern Optics*, 1994, **41**, 209.
25 M. G. Moharam and T. K. Gaylord, *J. Opt. Soc. Am.*, 1981, **71**, 811.
26 J. Muller, A. Herman, A. Mayer and O Deparis, *Opt. Expr.*, 2015, **23**, A657.
27 S. G. Johnson and J. D. Joannopoulos, *Opt. Expr.*, 2001, **8**, 173.
28 J. M. Bendickson, J. P. Dowling and M. Scalora, *Phys. Rev. E.*, 1996, **53**, 4107.
29 O. Deparis, *Opt. Lett.*, 2011, **36**, 3960.
30 M. K. I. Senevirathna, P. K. D. D. P. Pitigala and K. Tennakone, Solar Energy Mat. & Solar Cells 2006, **90**, 2918.
31 Y. Bessekhouad, D. Robert and J.-V. Weber, Catal. Today, 2005, **101**, 315.
32 D. Ke, H. Liu, T. Peng, X. Liu and K. Dai, Mat. Lett., 2008, **62**, 447.